Ordinary and Extreme Statistics of hourly water level and significant wave height observations at Ancona (Adriatic Sea)

Renato Vitolo[1], Nazario Tartaglione[2]

PASEF Group - University of Camerino

1) Department of Mathematics and Informatics

2) Department of Physics

Abstract

This work analyzes the statistics of time series of water level and significant wave height recorded at Ancona, Italy, by a tide gauge and a buoy, respectively, during the period 2000-2005. Beyond standard statistical analysis, extreme value statistics is examined.

Ancona is an interesting site because the amphidromic point for the M2 (i.e., the lunar semidiurnal) constituent lies nearby, making this constituent secondary with respect the diurnal one. Since the M2 component is the largest in the Adriatic Sea, the analysis of data without this component can give a better understanding of behaviour of other tidal constituents as well as non-tidal components.

The study of the water level and the significant wave height is of great interest for defining the coastline.

1. Introduction

It is customary nowadays, in tidal heights analysis, to use hourly values of surface elevation obtained from a digital tide gauge. The values recorded by these gauges are the result of interaction between astronomical tides and fluctuations due to sea currents and meteorological events.

The analysis and prediction of tides in the Adriatic Sea is the subject of many studies (e.g. Polli, 1959; Defant, 1961). In the last years such studies have been limited to northern Adriatic Sea, where the sea elevation reaches the maximum amplitude (e.g. Malacic et al., 2000; Lionello et al., 2005). The Adriatic Sea is a marginal sea and the classical astronomical tide theory does not work. Tidal effects occur as a side-effect of the sea level variability of the Mediterranean trough shallower water as combinations of incident and reflected Kelvin and Poincaré waves (Taylor, 1921). Hendershott and Speranza (1971) revisited the Taylor theory and showed that in the analyzed semi-closed basins all Poincaré modes are evanescent and the partial reflection of the Kelvin wave causes a displacement of the M2 amphidromic point from the channel axis toward the western coast. Moreover, other constituents may have their amphidromic point out of the sea (inland), making it virtual.

The M2 amphidromic point for the Adriatic Sea lies right off Ancona and, therefore, the behaviour of the tide at Ancona is particularly interesting with respect to other Adriatic sites. Simulating the tide in an Adriatic location is not simple for the reasons mentioned above. Additional non-astronomical factors such as configuration of the coastline, local depth of the water, ocean-floor topography, and other hydrographical and meteorological factors may play an important role in altering the range and times of arrival of tides.

The knowledge of water level is important for different reasons, among these the evolution of beaches. The dissipation energy per volume unit caused by sea action on a beach is given by $D=\sqrt{h}\frac{dh}{dy}$, where h is the water level and y is the coordinate going from the sea to land (across the shoreline). If we assume that D is a constant, increasing h, dh/dy must decrease and the shoreline retreats.

On the other hand, the knowledge of fluctuations of high and low water is necessary to define tidal datum, although for a correct definition of such datums observations taken over 19 years are needed. For marine applications, a vertical datum is defined as a base elevation used as a reference from which to determine relative heights or depths. It is called a tidal datum when defined by a certain phase of the tide. Tidal datums are local datums and should not be extended into areas which have differing hydrographic characteristics without substantiating measurements. The application areas of tidal datums are manifold, from coastal management to emergency management; for defining the legal boundaries of a country or to help defining the nautical charts.

An important aspect concerning sea level is the analysis of extreme values. Extreme values are of great importance from an economical point of view. Since sea defences can be built only knowing return time associated with extreme recorded values. A point process model has been used for the inference of extreme values. It requires a procedure based on *threshold exceedances*. This method is applicable under very general conditions. It is reliable and flexible, thus quite suitable for the

formulation of standards. Moreover, such a method allows accurate estimation of risk. For example, *flood risk* can be quantified in a straightforward way as a *return period* associated to a given return level.

2. Water level data

For this report, hourly data are used, gathered from the Ancona station (Fig. 1) for the period 2000-2005. The time series of observed water level, running from the 1st January 2000 to 31st December 2005, is shown in Fig. 2.

The data for this station are provided by the "Agenzia Nazionale per la Protezione dell'Ambiente e per i Servizi Tecnici (APAT), which manages a network of buoys and tide gauges whose observations are made available through Internet (http://www.idromare.com) and other media.

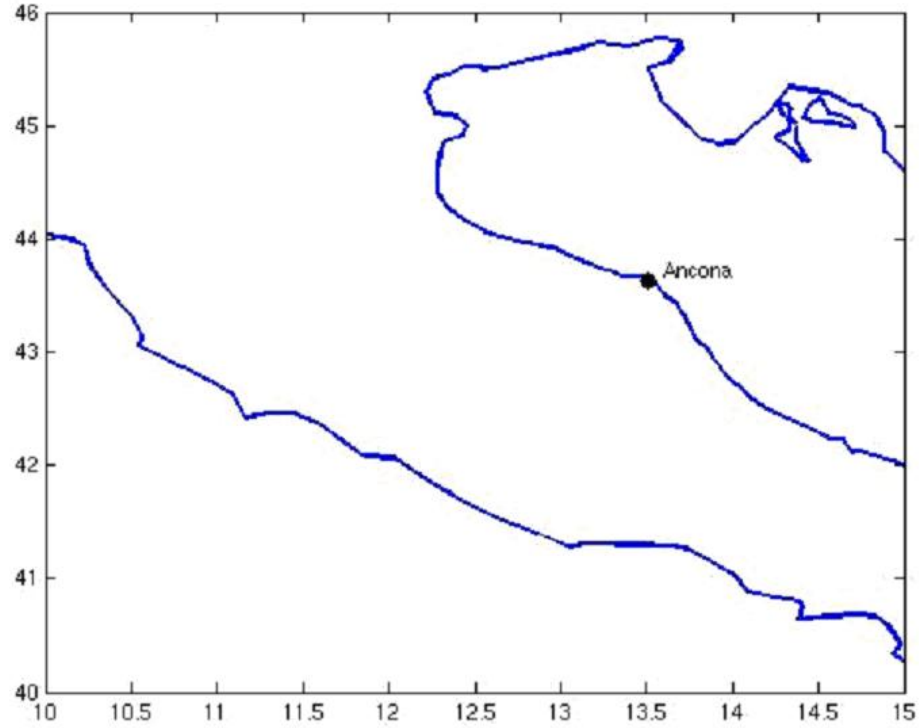

Fig. 1. The Adriatic basin and the location of Ancona tide gauge.

Tide gauges record water level. Although the water level series are available on the web site from 1986, there are several periods with missing data. Also, the time series from 2000 to 2005 have very few missing observations. A quality check was performed and the missing data were replaced by a linear interpolation between the previous and the next values. If a spike was found, again it was replaced by a linear interpolation between two contiguous sea levels.

The statistics characterizing these observations as a function of year are listed in Table 1. The mean value is always negative indicating a possible bias for the gauge; moreover it changes during the years. This means that we can define only a yearly

mean sea level. In order to define the Mean Sea Level as a tidal datum, a period of 18.6 years should be considered, since it is the period of nutation. Too little data are available to allow for the above definition of trend, so that no appreciable change may be reliably inferred during the considered period (Fig. 3, Tab.1).

Table 1. Statistics of observations as a function of year at Ancona

Year	Number	Mean	Std Dev
2000	8784	-0.05317	0.179646
2001	8760	-0.01191	0.162019
2002	8760	-0.02375	0.183347
2003	8760	-0.05606	0.180090
2004	8784	-0.03226	0.178699
2005	8760	-0.05476	0.174413

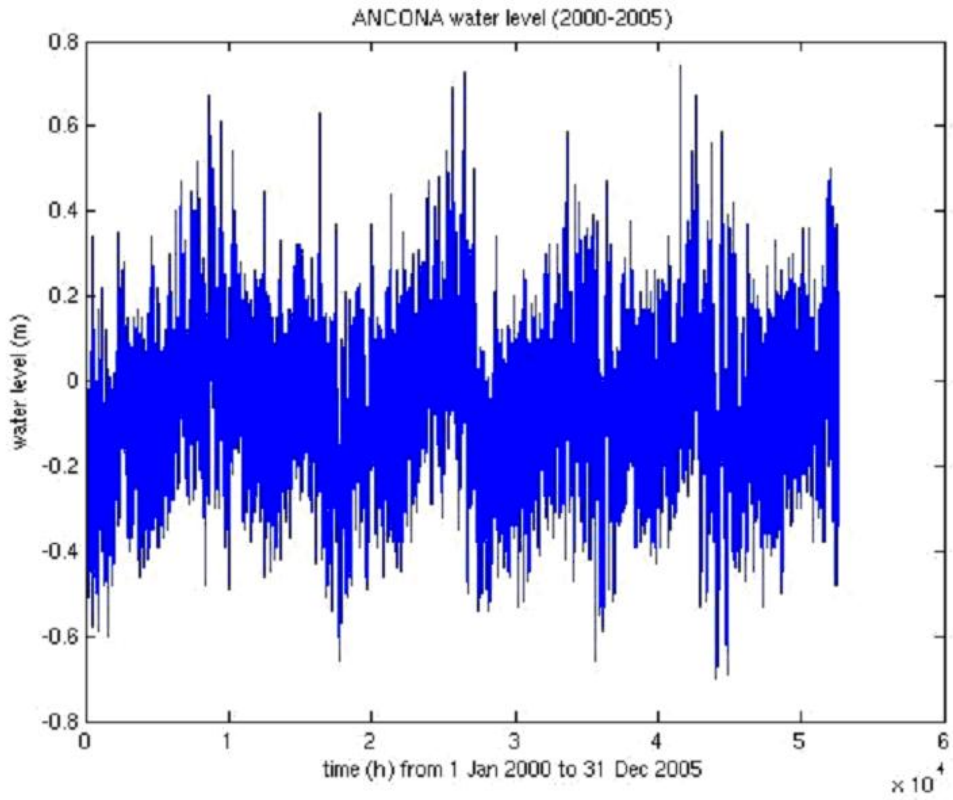

Fig. 2. Time series of water level observations from 1st Jan 2000 to 31st Dec 2005.

Figure 3 shows oneway analysis of observed water level by month. It is worth noting that the observed annual cycle might be associated with the position of the Earth with respect to the Sun. On the other hand, the overall variability, which is associated to the variability of residuals, is mainly caused by meteorological effects, which are maximal during the autumn and winter season (see Fig. 4). Many occurrences of water levels higher and lower than 99th percentile, indicated by the upper and lower limits of bars, occurred from September to March.

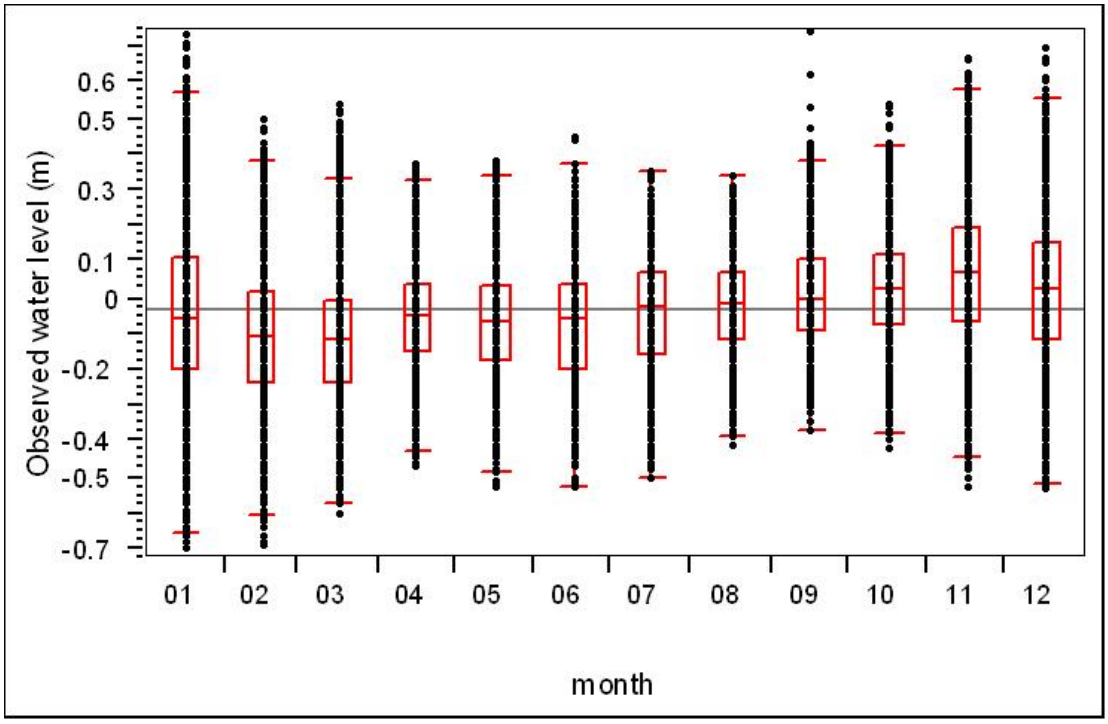

Fig. 3 Oneway analysis of observed water level (m) by month. In this figure, also the median is shown, as well as the 10^{th}, 25^{th}, 75^{th} and 90^{th} quantiles.

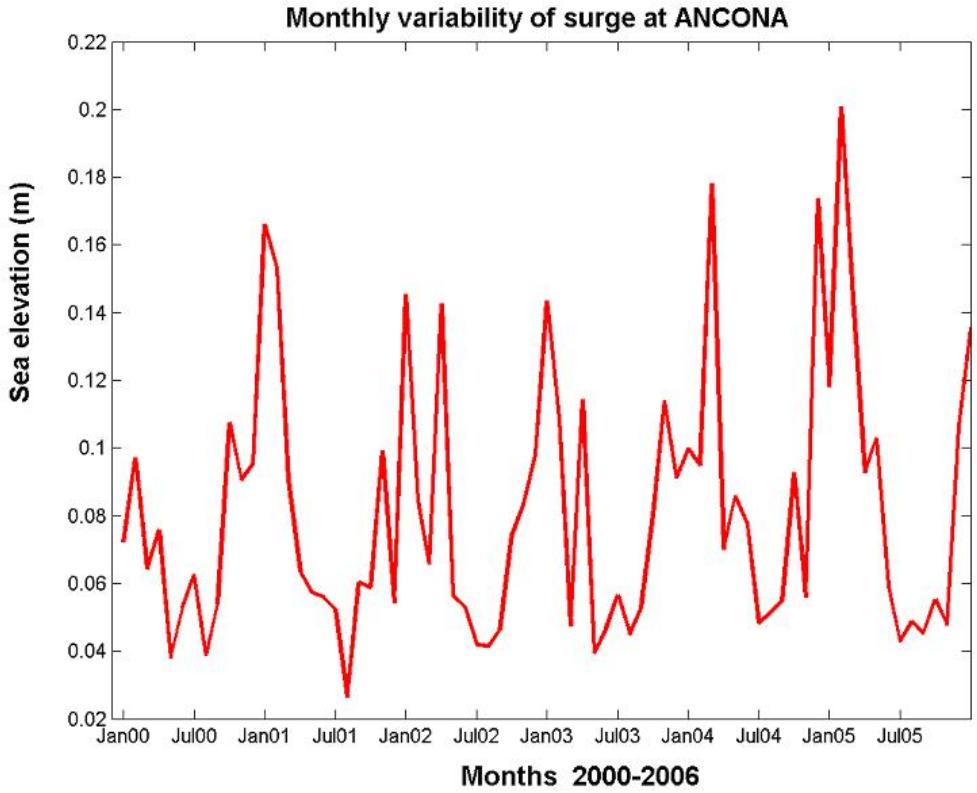

Figure 4. Monthly standard deviation of residuals at Ancona.

3. Harmonic and spectral analysis

In classical harmonic analysis, the tidal forcing is modeled as a set of spectral lines, i.e., the sum of an infinite set of sinusoids at specific frequencies. These frequencies are specified by various combinations of sums and differences of integer multiples of some fundamental frequencies arising from planetary motions (Godin, 1972). A least-squares fit can be used to determine the relative phase and amplitude of each frequency in the response. This phase/amplitude data thus provides a compression of the data in the complete time series, which can then be compared with similar data at other locations to understand the characteristics of tidal dynamics, or can be used to synthesize time series of tidal effects at other times for predictive purposes.

There are several drawbacks to classical harmonic analysis. The first is that, ignoring the modulation of perihelion, which is effectively constant over historical time, about 18,6 year time series is required to resolve all of the listed frequencies (that is, the number of wavelengths of each constituent in the record differs by at least 1 unit from all other constituents). In practice, record lengths are often 1 year or shorter. In order to handle this issue an assumption is made that the phase/ amplitudes of response sinusoids with similar frequencies are in the same proportion as those of the equilibrium response under the reasonable premise that the ocean response should

be similar at similar frequencies. In such a cluster, large equilibrium peaks are surrounded by small subsidiary peaks in frequency space which provides ‘‘nodal modulations’’ (or more correctly, ‘‘satellite modulations’’) to the main peak.

The appearance of the total signal will be a sinusoid whose phase and amplitude varies slowly with time. These changes are slow enough to be considered effectively constant for record lengths of up to 1 year.

At much shorter record lengths another problem arises. The frequency resolution further degrades until even dissimilar constituents are irresolvable. The best solution is to apply inference. This technique for finding the absolute phase/amplitude requires that the relative differences in phase/amplitude between the two unresolved constituents is known from other nearby data. If this is not the case, it is thought best to either discard the smaller constituents or only fit to the largest in a given frequency interval, or to use the equilibrium response to establish the desired differences.

Another drawback of classical analysis is that it provides no easy way to determine whether the resulting phase/amplitude of a given sinusoid is meaningful in a deterministic way (i.e., it is truly a tidal line), or whether it results from fitting to a component of the non-tidal broad-spectrum variability. In general a fit is likely to include elements of both and some kind of confidence interval for the deterministic part is useful. To address this issue, the ‘‘response’’ method was invented (Munk and Cartwright, 1966). Although this provides better results than classical harmonic analysis, it has not found widespread use.

Further problems with classical harmonic analysis arise in coastal regions where the tidal response is in the form of a wave propagating onshore. In large estuaries, the seasonal change in salinity and flow may change the dynamic response but as these changes can vary from year to year, the tidal process is not stationary.
Instead, spectral peaks are broadened so that they are no longer pure lines, but, depending on the situation, such variations may be treated as lines in the analysis. Within smaller estuaries, tidal height variations may be significant compared to water column depth and a variety of non-linear effects can occur. For example, floods in general shorten and intensify the rising tide, whereas ebbs get longer. As long as these effects are reasonably deterministic they may be handled by adding extra ‘‘shallow water’’ constituents which occur at sum/difference frequencies of the major constituents.

More problematic in these regions are the effects of internal variability. Tidal interactions with varying topography can produce large internal waves and bores whose characteristics are highly sensitive to ambient stratification. In such cases the assumption of ‘‘line’’ frequencies becomes questionable and other techniques such as wavelet analysis have been suggested (Jay and Flinchem, 1999). More comprehensive descriptions of analysis techniques their uses and limitations are given in, e.g., Foreman et al. (1995) and Godin (1991).

The data recorded by tide gauges $D(t)=T(t)+M(t)$ are a sum of a tidal signal $T(t)$ (with m tidal constituents) plus a non-tidal signal $M(t)$. The response of water to non-tidal forcing may have periodic constituents that are not strictly associated with tides. For example, current driven by breezes, normal modes associated with the oscillations of basin (seiches), impact of different kinds of wind that occur with seasonal frequency and radiative effects on sea water, can give a sort of periodicity to water level that is not dependent on tide causes. Thus the signal $M(t)$ could also have

periodic constituents.

We are interested in analysis both tidal and extra-tidal constituents. The analysis has been performed by means of tidal analysis software (Pawlowicz et al., 2002) derived from an algorithm developed by Godin (1972) and Foreman (1978). Moreover, we have analyzed the periodic behaviour trough the classical spectral analysis and by means of spectral analysis. Results are shown in Fig. 6: the diurnal constituent is the highest one. The annual constituent shows a higher value than other constituents but the K1 and M2.

Zooming on higher frequencies and lower period (Fig. 5), we can note that together to the 24 hour component, there are near components with an appreciable power density. These components are not associated with seiches, as it will be seen later. After eliminating the contribution of tidal constituents found by the t_tide software we have looked through the residual frequencies to see if an important signal is present in the spectrum.

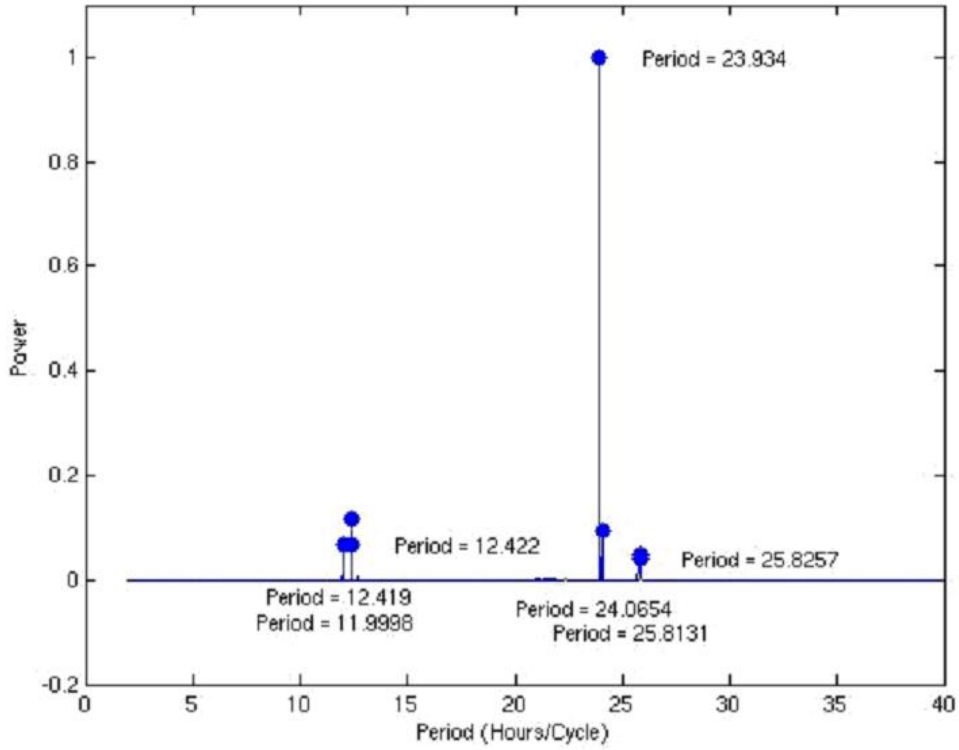

Figure 5. Tidal high frequency components at Ancona. It is worth noting the strong diurnal component, differently from the observed ones at other stations such as Venice, where the predominant component is the semidiurnal one.

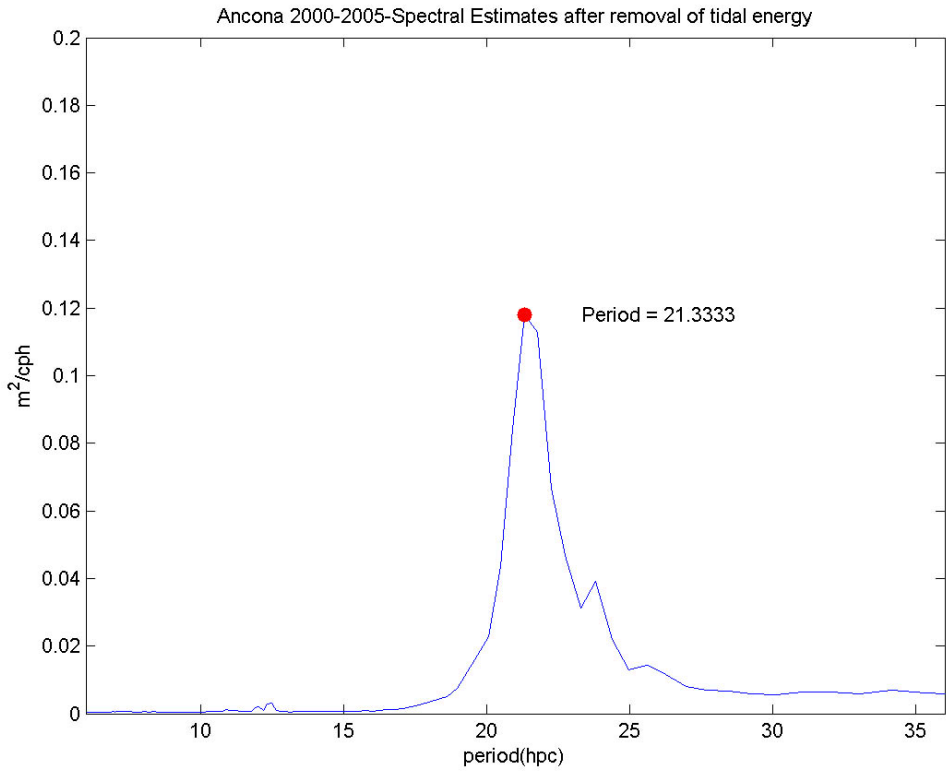

Figure 6. Power spectral density of the residuals as seen at Ancona. The first component of seiches is indicated.

4. Seiches

At higher frequencies it is possible to see the presence of seiches. The contribution to total spectrum is not very high. As opposed to tidal constituents, seiches occur only several times in a year as a response of sea to meteorological forcing from the south boundary of the Adriatic. The oscillation of seiches is important above all on the northern Adriatic that represents the head of the basin. Numerical simulations of tide for the Adriatic (Lionello et al., 2004), showed that the amplification factor of the seiches at Ancona is close to 1 whereas at Venice it is larger (1.4).

The spectral power density of the seiches components is shown in Fig. 6, as obtained by first removing the tidal constituents and then using the Welch's PSD estimation. The first oscillating normal mode, having a period between 21 and 22 hours has stronger power spectral density than the second normal mode.

5. Point process approach applied to water level

For the statistical analysis of extreme values, one has to deal with the non-stationarity of the data, due to the seasonal cycle. The most straigthforward way is to perform inference on the sequence of the yearly maxima extracted from the time series: this is the so-called *annual maximum* method, which relies on the Generalized Extreme Value (GEV) distribution. A problem with this approach is that one is

discarding most of the available data: if the data record is short (as it is the case for all time series analyzed here), the resulting GEV parameter estimates have very large uncertainties and are unreliable for practical purposes, especially for computation of return levels (which requires extrapolation to large values). An alternative and very fruitful approach is to use the so-called point process modelling, which is based on the following theorem: let be a sequence of independent and identically distributed random variables and define

$$N_n = \{(i/(n+1), X_i) : i = 1, \ldots, n\}. \quad (1)$$

Then, for sufficiently large u and in the limit $n \to \infty$, on regions of the form $(0,1)\times[u,\infty)$, is approximately a Poisson process, with intensity measure on given by

(2)

In this framework, time-dependence (non-stationarity) of the time series is modeled in a straightforward manner: time-dependent parameters $(\mu(t),\sigma(t))$ and threshold $u(t)$ are chosen, whereas ξ is kept constant to avoid numerical convergence problems. In this report, to model seasonal variability, we adopt the following choices for the point process model: a threshold

$$u(t)=a+b\sin(2\pi(t-d)/365.25) \quad (3)$$

and time-dependent GEV parameters $(\mu(t),\sigma(t))$ given by

(4)

and

(5)

with constant ξ. Therefore, the parameter vector to be inferred from the data is

(6)

A maximum likelihood method is used for the inference of these parameters: in fact, by a suitable normalization of the likelihood function one obtains that the parameters μ_0, σ_0, ξ of the stationary point process given by are those of the annual maximum GEV distribution, see Coles (2001). In the following analysis, this stationary model is used as well and yields reasonable inferences. However, given the strong periodic component in the residual time series, it is appropriate to take periodicity into account in the statistical model. This is also confirmed by by means of the *likelihood ratio test* (Coles, 2001). Lastly, sensitivity studies are regularly performed to assess the robustness of the threshold choices.

To apply the point process model, first the daily maxima of the time series are computed; the resulting sequence of daily maxima is used as basis for the inference. Using a constant threshold u=0.4, one has 45 threshold exceedances (see Fig. 7 top, left and center panels). However, the correlation is not very low (Fig. 7 top, right panel). Using a stationary point process model with the above threshold yields the

estimates in Tab. 2 (top row) for the GEV parameters of the annual maximum distribution. Notice that the point estimates are very similar to those obtained by straightforward GEV inference (not shown here), but the uncertainties are much smaller (particularly so for the parameter ξ), due to the fact that a considerably larger fraction of the available data is being used. However, the diagnostic plots (Fig. 8 top) reveal that the fit is not quite accurate. Using a threshold value of 0.3 yields similar estimates (Tab. 2, bottom row) and the diagnostic plots (Fig. 8 bottom) look somewhat more reassuring. Choosing lower values for the threshold yields increasingly more correlation in the sequences of exceedances and should be avoided.

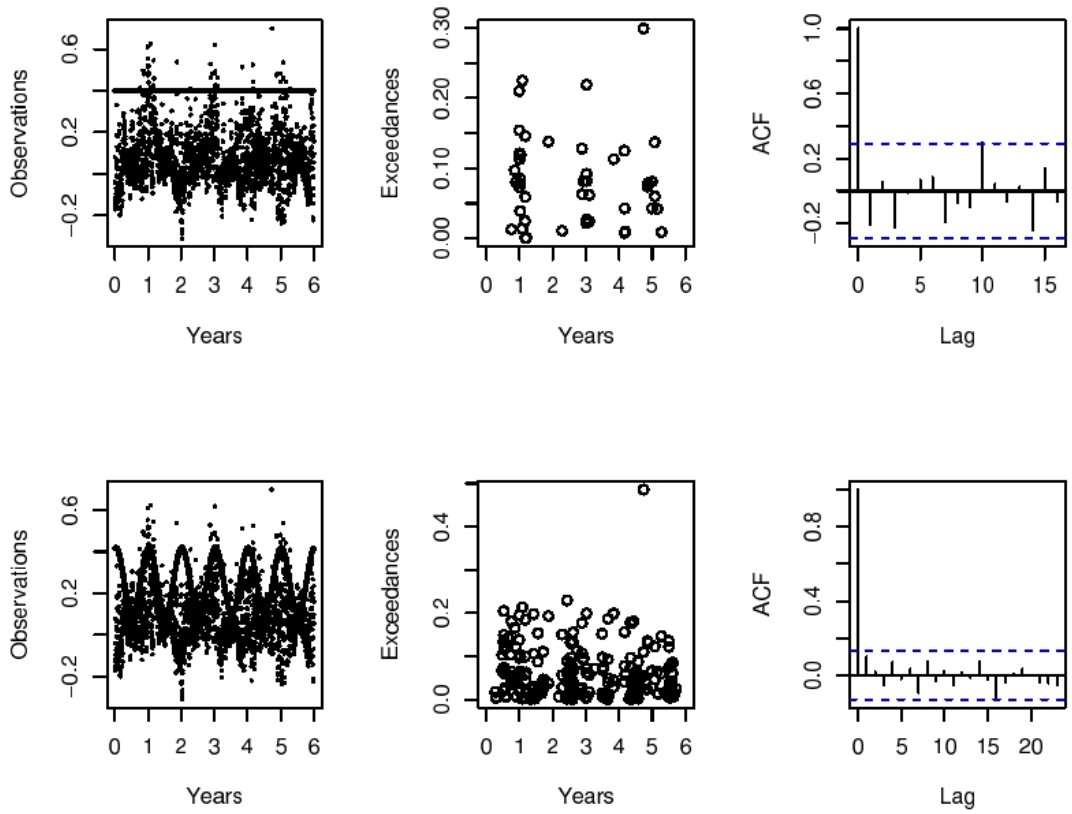

Figure 7: Top, left panel: a constant threshold u = 0.4 (compare with Tab. 2, top row) is applied to the sequence of the daily maxima extracted from the time series in Fig. 2. The sequence of threshold exceedances and their autocorrelations are plotted in the center and right panel, respectively. Bottom: same as top for the time-dependent threshold in (3), with parameters as in (7).

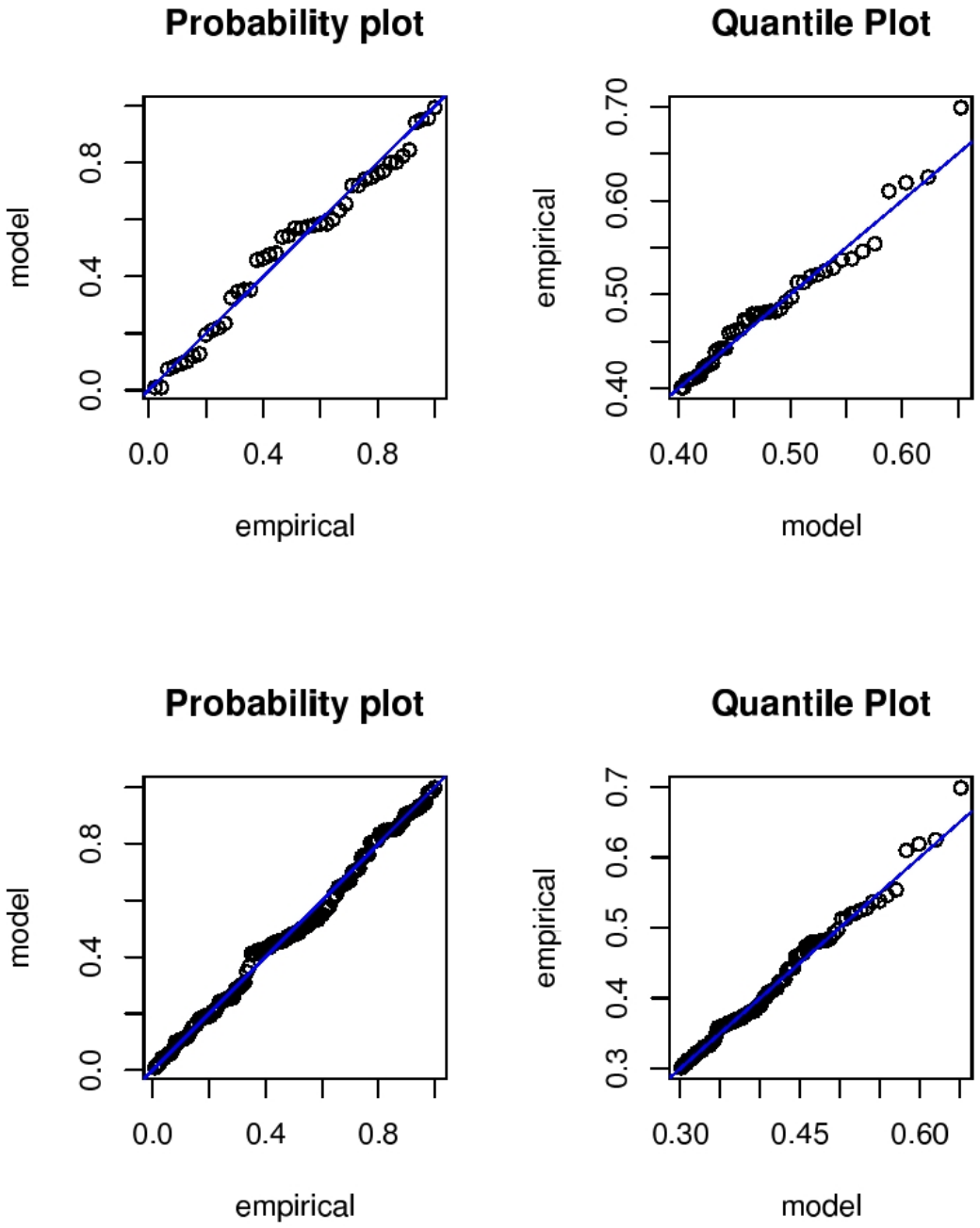

Figure 8: Top, bottom: diagnostic plots of the stationary point process inferences in Tab. 2 top and bottom, respectively.

u	n. exc.						
0.4	45	0.563	0.021	0.062	0.009	-0.26	0.122
0.3	123	0.559	0.019	0.062	0.009	-0.21	0.076

Table 2: Maximum likelihood estimates (,,) of the GEV parameters inferred by stationary point process modeling from the sequence of daily maxima of the hourly time series in Fig. 2. The associated standard errors have been computed by the observed information matrix. The threshold value *u* used to select the extreme values used for the inference and the number of exceedances above the threshold are

reported in the first and second column from left, respectively. Diagnostic plot for the inference in the top row are given in Fig. 8.

0.589	0.041	0	0	0	0
-2.246	0.243	0	0	0	0
-0.056	0.083				

Table 3: Maximum likelihood estimates of the parameter vector (6) of a stationary point process model, inferred from the sequence of daily maxima of the hourly time series in Fig. 2. The time-dependent threshold $u(t)$ as in (3) used to select the extreme values is reported in (7). The maximized log-likelihood is 880.3.

0.484	0.019	0.031	0.007	0.157	0.006
-2.798	0.176	0	0	0	0
-0.007	0.062				

Table 4: Same as Tab. 3 for a point process model with μ depending on time as in (4) and constant σ. The maximized log-likelihood is 990.7.

0.497	0.023	0.025	0.024	0.205	0.022
-2.769	0.179	-0.028	0.103	0.208	0.088
-0.019	0.062				

Table 5: Same as Tab. 4 for a point process model with both μ and σ depending on time as in (4)-(5). The maximized log-likelihood is 993.4.

The time-dependent threshold (3) is then applied, with

$$(a,b,d)=(0.26,0.16,-80), \qquad (7)$$

yielding 225 exceedances. The threshold is plotted together with the data in Fig. 7 bottom, left panel. The distribution of the exceedances shows non-stationary behaviour (Fig. 7 bottom, center panel), particularly when compared with the constant-threshold selection (Fig. 7 top, center panel). However, the selected exceedances are less correlated (Fig. 7 bottom, right panel) than in the constant-threshold case (Fig. 7 top, right panel). Three different point process models are inferred on the above exceedances: a stationary model, a model with time-dependent μ but constant σ, and a model with time-dependent μ and σ. The obtained inferences are reported in Tab. 3, Tab. 4, and Tab. 5, respectively. An exponential link function has been used in the model for the parameter σ, to ensure its positivity. This explains the negative values obtained: in fact, the value $\exp(-2.77)\approx 0.063$, which is again similar to that inferred with the stationary point process with constant threshold (Table 2). However, the point estimate of ξ is rather different from those obtained by the stationary point process model. One may conclude that disregarding the seasonal component of the signal induces too small (negative) estimates for ξ, since the distribution of the selected extreme values "looks" more sharply bounded from above than when using a time-dependent threshold. In fact, the smallness of the absolute value of ξ for the time-dependent point processes inferred in Tab. 4 and Tab. 5 suggests that a straight Gumbel fit ($\xi=0$) might be appropriate as well. Diagnostic plots for the three inferences are given in Fig. 9. These confirm that the stationary fit is not adequate, whereas there is no sensible difference in the two fits with time-periodic μ and constant or time-periodic σ (also, the maximized log-likelihoods in these two cases are rather similar).

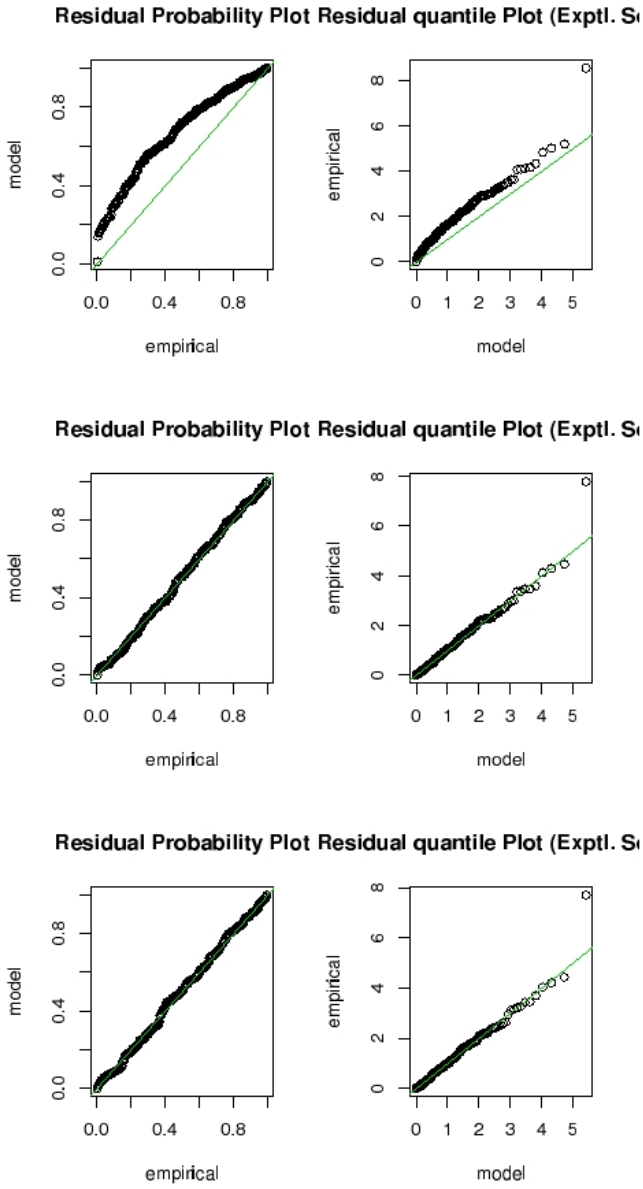

Figure 9: From top to bottom: diagnostic plots for the point process inferences reported in Tab. 3, Tab. 4, and Tab. 5, respectively.

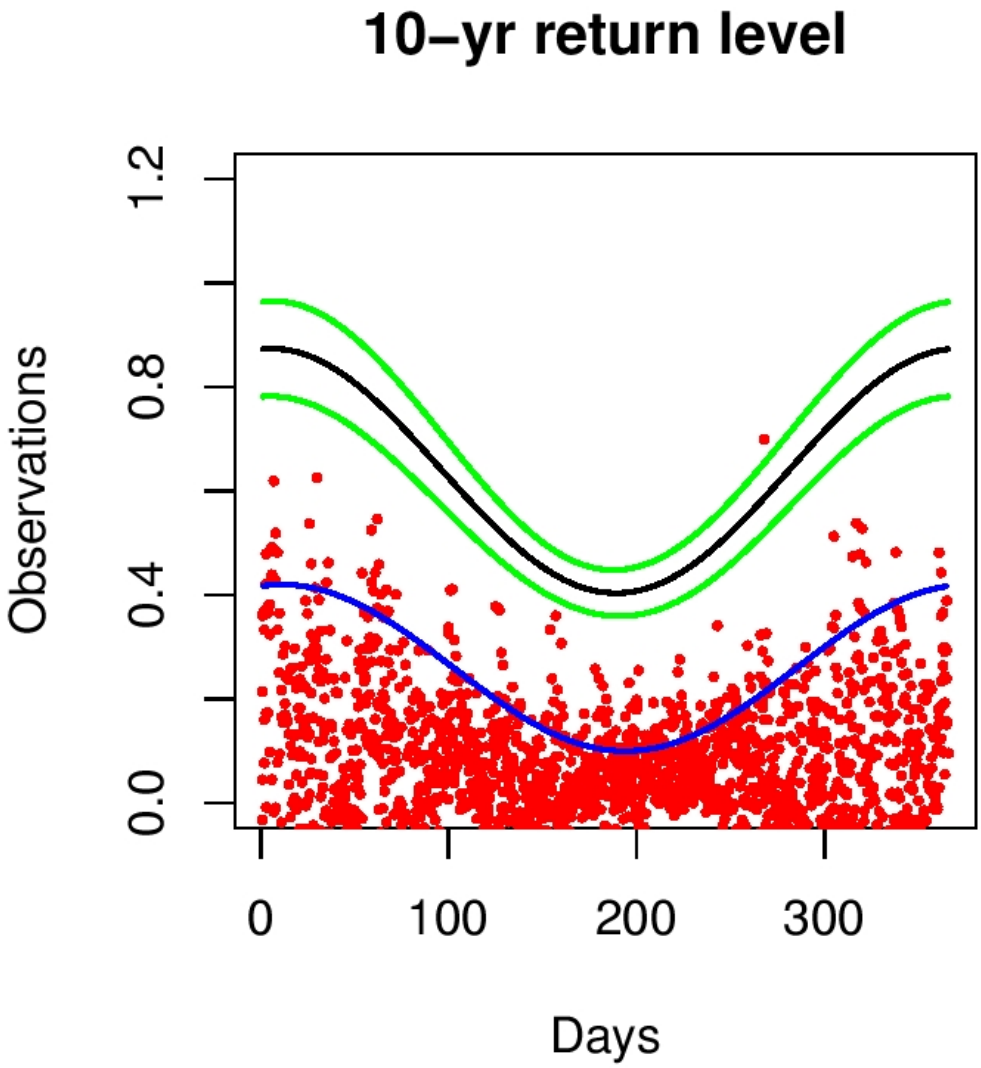

Figure 10: Seasonally-varying 10-year return level of the surge at Ancona (black) plus σ -confidence interval (green). In red, the sequence of daily maxima of the hourly time series in Fig. 2 is plotted, together with the time-dependent threshold (3) (blue), whose coefficients are given in (7).

To compute return levels, we choose the GEV model in which both μ and σ have seasonal dependence on time, that is, Eqs. (4) and (5) hold with parameter vector (6) given by the estimates in Tab. 5). The return levels of the surge also have seasonal dependence on time: point estimates might be easily obtained via the following formula for the quantiles of the GEV distribution:

(8)

for ≠0 and

(9)

for =0. However, this approach would not provide a measure of uncertainty. To obtain

this, we resort to simulation. The maximum likelihood procedure for the estimation of the parameter vector (6) also yields a covariance matrix *M* (from which the uncertainties in Tab. 5) are computed). Under reasonable assumptions (Coles, 2001) the maximum likelihood estimator is asymptotically multinormally distributed. So we generate a random sample of values of the parameter vector (6), multinormally distributed and with covariance matrix given by *M*. For each realization of the sample, the quantities $\mu(t)$ and $\sigma(t)$ are computed by Eqs. (4) and (5) for *t* fixed and substituted in (8) or (9) with $1/p$=10 years, yielding a value which depends on the time *t* of the season. Then, mean and variance of the obtained sample of are computed. This is repeated for values of time *t* belonging to a grid covering a time span of one year. The results are plotted in Fig. 10: in wintertime, the expected 10-year return level is larger than in summer and so is the related uncertainty.

6. Waves

Strong winds on the surface of a body of water will cause sea waves that can affect the water level. A buoy is moored off Ancona. It records the significant spectral height of the wave motion with associated average incoming direction, taken at buoys belonging to the "Rete Ondametrica Nazionale" (RON). Until 31/12/2001, the data is recorded every three hours, except when a value of the significant wave height is detected above the threshold of 3m, in which case data is measurements are acquired every half hour. Since 1/1/2002 all measurements are recorded every half hour. The timespan of the time series ranges from 1/1/1999 to 31/12/2004. We show the scatterplot the wave heights with tide measurements and the wave heights with surge (Fig. 11).

It can be noted that at distribution of point corresponding at high value wave height is elongated towards high values of sea level, even though a linear relationship is hard to be found. Strangely, when only residuals are plotted versus significant height of wave, the relationship high wave height equal high values of sea level, due to residuals, is not so clear, at first glance. On the other hand, there is a clear relationship between variability of residuals and seasons (fig. 4), that determines seasonal variability of sea level.

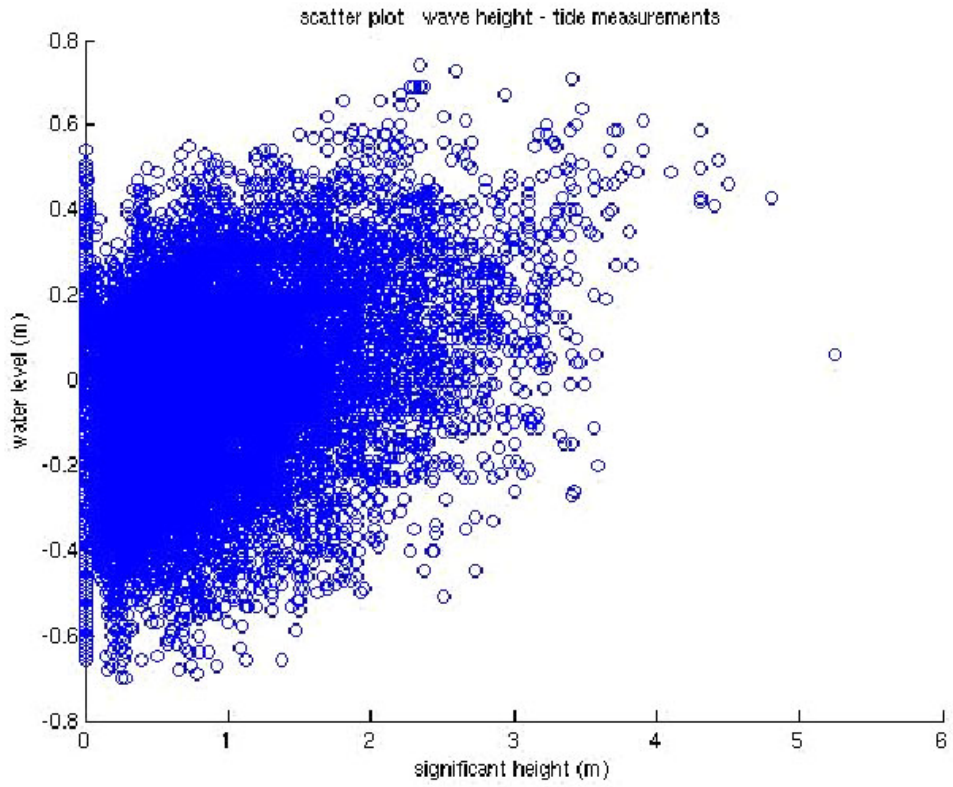

Figure 11. Scatterplot of significant wave heights and sea levels at Ancona

3.2.1 Point process estimation of extreme values of waves

The data analyzed in this section are measurements described in the above subsection. As the analysis performed on the water level, at first, the daily maxima of the significant wave height are computed, independently of the average incoming direction. The resulting time series of length 6 years is used as basis for the statistical inference. It is to be noted, however, that the time series is characterized by absence of observations in several portions of the record, in certain cases for many consecutive days. Moreover, several *spikes* (that is, erroneously large values) were present and have been removed from the time series.

A plot of the daily maxima of the significant wave height in the considered timespan is given in Fig. 12.

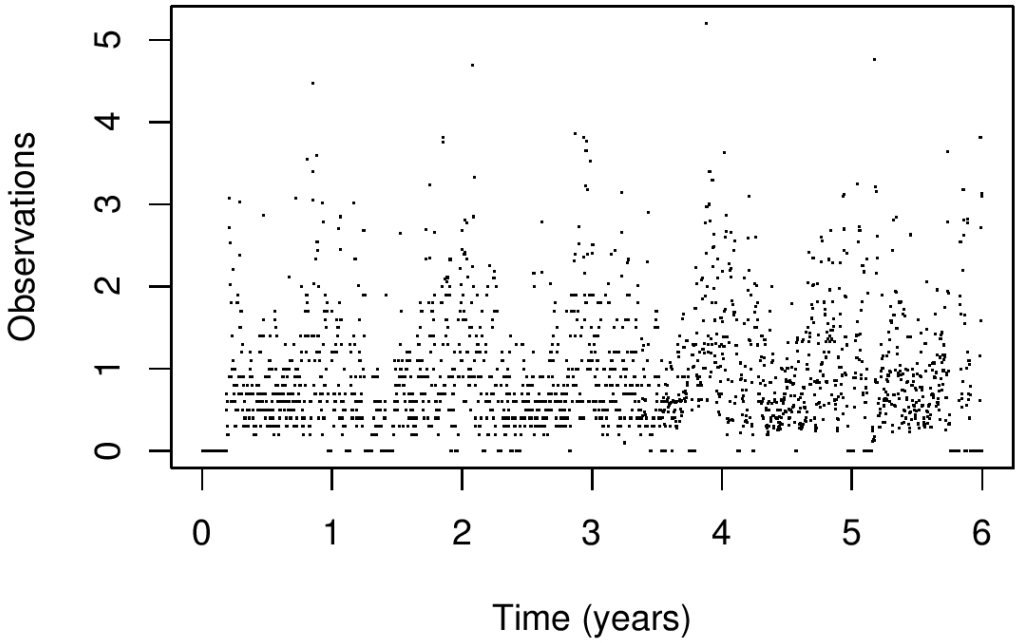

Figure 12: Time series of the daily maxima of the significant spectral wave height at Ancona RON site during the years 1999-2004.

As in the previous section, we resort to point process modeling, since the numerical procedure of GEV for the annual maxima even fails to converge (not shown) due to data scarcity: only 6 yearly maxima are available, which would yield unreliable estimates anyway.

We first adopt the stationary model: a constant threshold u=2.5 is first selected, above which there are 94 exceedances (Fig. 13 top, left and center panels). The correlation is not very low (Fig. 13 top, right panel). The inference of a stationary point process model with the above threshold is reported in Tab. 6 (top row). The diagnostic plots (Fig 14, top row) indicate that the fit is reasonably good, though not accurate at the upper tail of the distribution (see the quantile plot). Choosing lower values for the threshold yields increasingly more correlation in the sequences of exceedances and should be avoided.

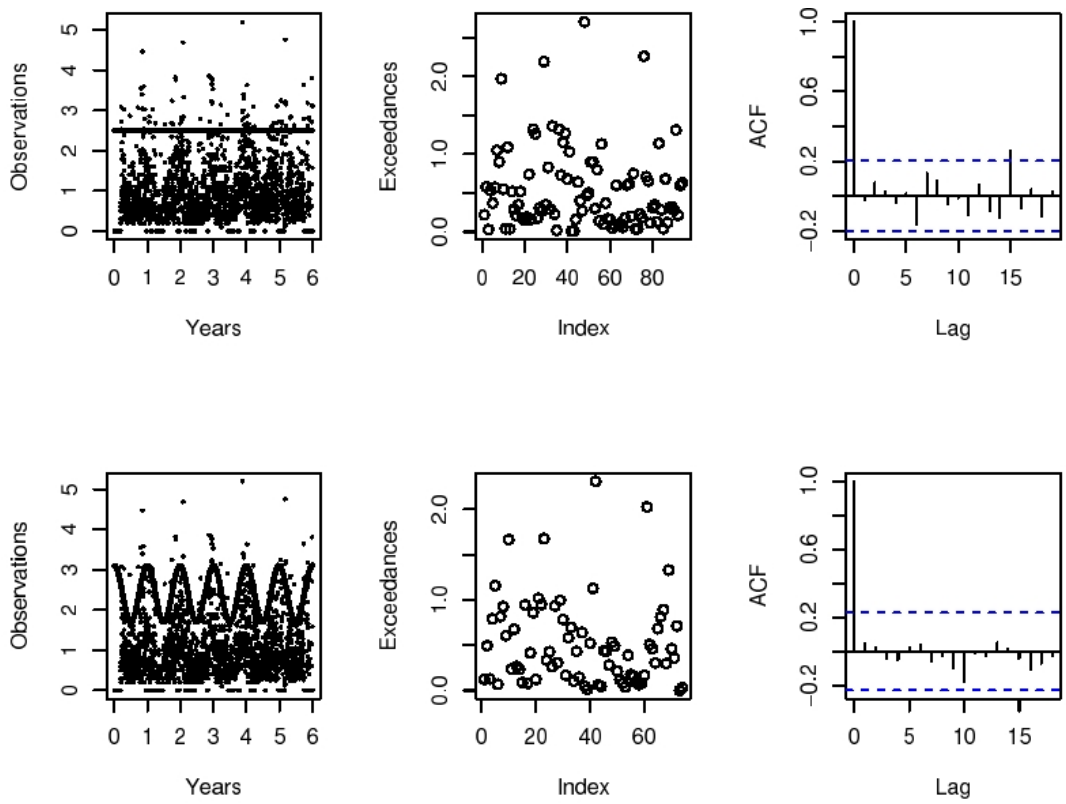

Figure 13: Top, left panel: a constant threshold u = 2.5 (compare with Tab. 6, top row) is applied to the sequence of the daily maxima extracted from the time series in Fig. 12. The sequence of threshold exceedances and their autocorrelations are plotted in the center and right panel, respectively. Bottom: same as top for the time-dependent threshold in (3), with parameters as in (10).

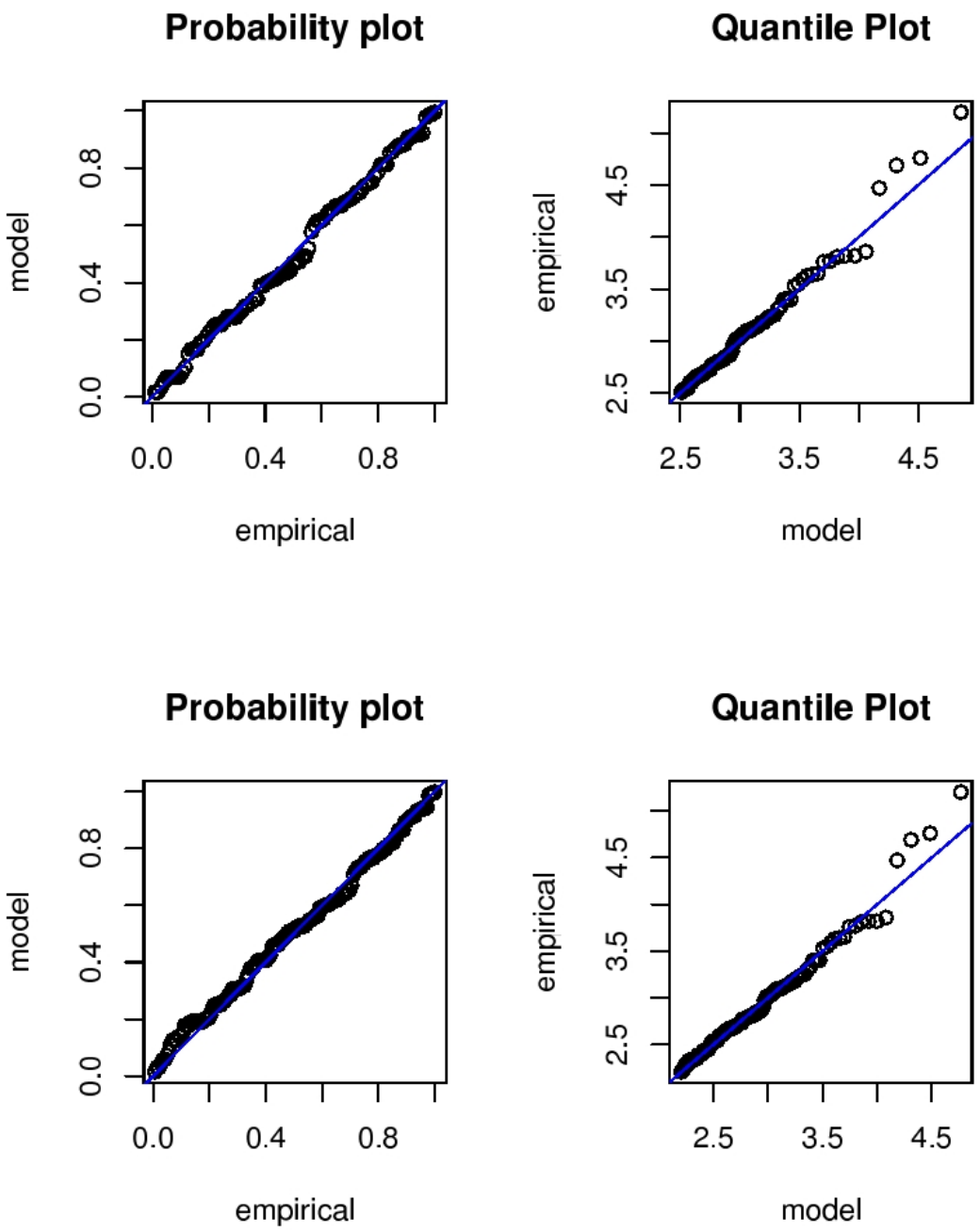

Figure 14: Top, bottom: diagnostic plots of the stationary point process inferences in Tab. 6 top and bottom, respectively.

u	n. exc.						
2.5	94	4.0	0.016	0.51	0.1	-0.03	0.1
2.2	142	4.0	0.15	0.47	0.08	-0.1	0.07

Table 6: Maximum likelihood estimates (,,) of the GEV parameters inferred by stationary point process modeling from the sequence of daily maxima of the time series in Fig. 12. The associated standard errors have been computed by the observed information matrix. The threshold value *u* used to select the extreme values used for the inference and the number of exceedances above the threshold are reported in the first and second column from left, respectively. Diagnostic plot for the inference in

the top row are given in Fig. 14.

The time-dependent threshold as in (3) is then applied, with

$$(a,b,d)=(2.4,0.7,-90), \qquad (10)$$

yielding 74 exceedances. The threshold is plotted together with the data in Fig. 13 bottom, left panel. The distribution of the exceedances looks quite independent on time (Fig. 13 bottom, center panel). Moreover, the selected exceedances are uncorrelated (Fig. 13 bottom, right panel). Three different point process models are inferred on the above exceedances: a stationary model, a model with time-dependent μ but constant σ, and a model with time-dependent μ and σ. The obtained inferences are reported in Tab. 7, Tab. 8, and Tab. 9, respectively. As in Sec. 5 an exponential link function has been used for the parameter σ. However, in this case the point estimates of ξ are not very different from those obtained with a constant threshold and a stationary point process model. Diagnostic plots for the three inferences of Tab. 7, Tab. 8, and Tab. 9 are given in Fig. 15. These confirm that the stationary fit is not adequate, whereas there is no sensible difference in the two fits with time-periodic μ and constant or time-periodic σ, both in the diagnostic plots and in the value of the maximixed likelihood.

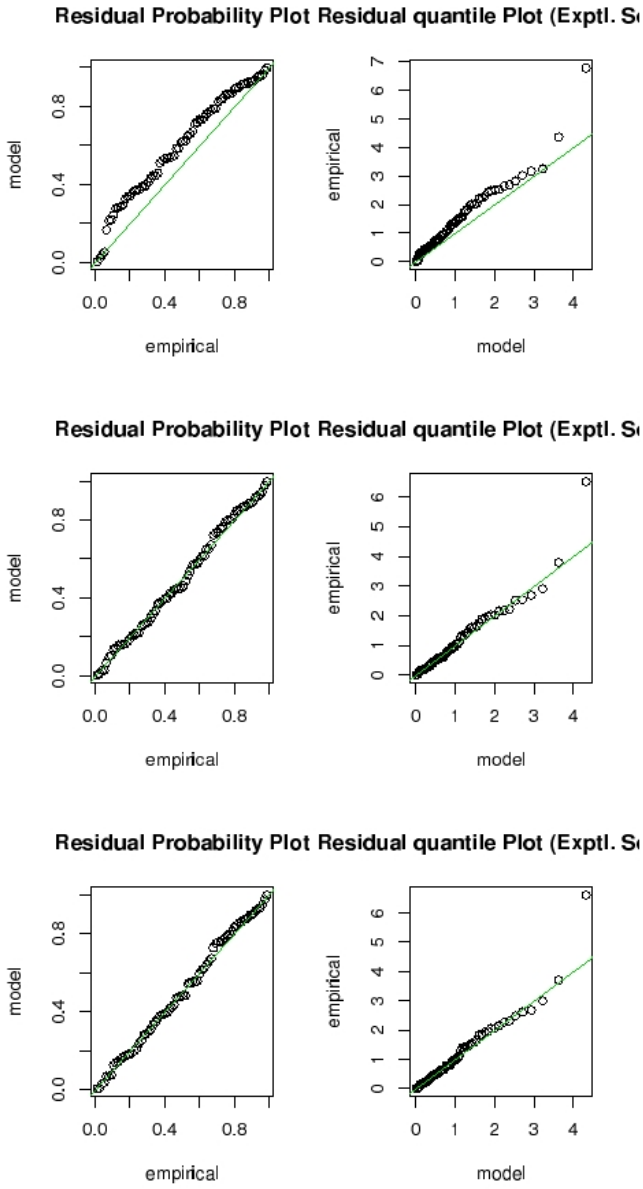

Figure 15: From top to bottom: diagnostic plots for the point process inferences reported in Tab. 7, Tab. 8, and Tab. 9, respectively.

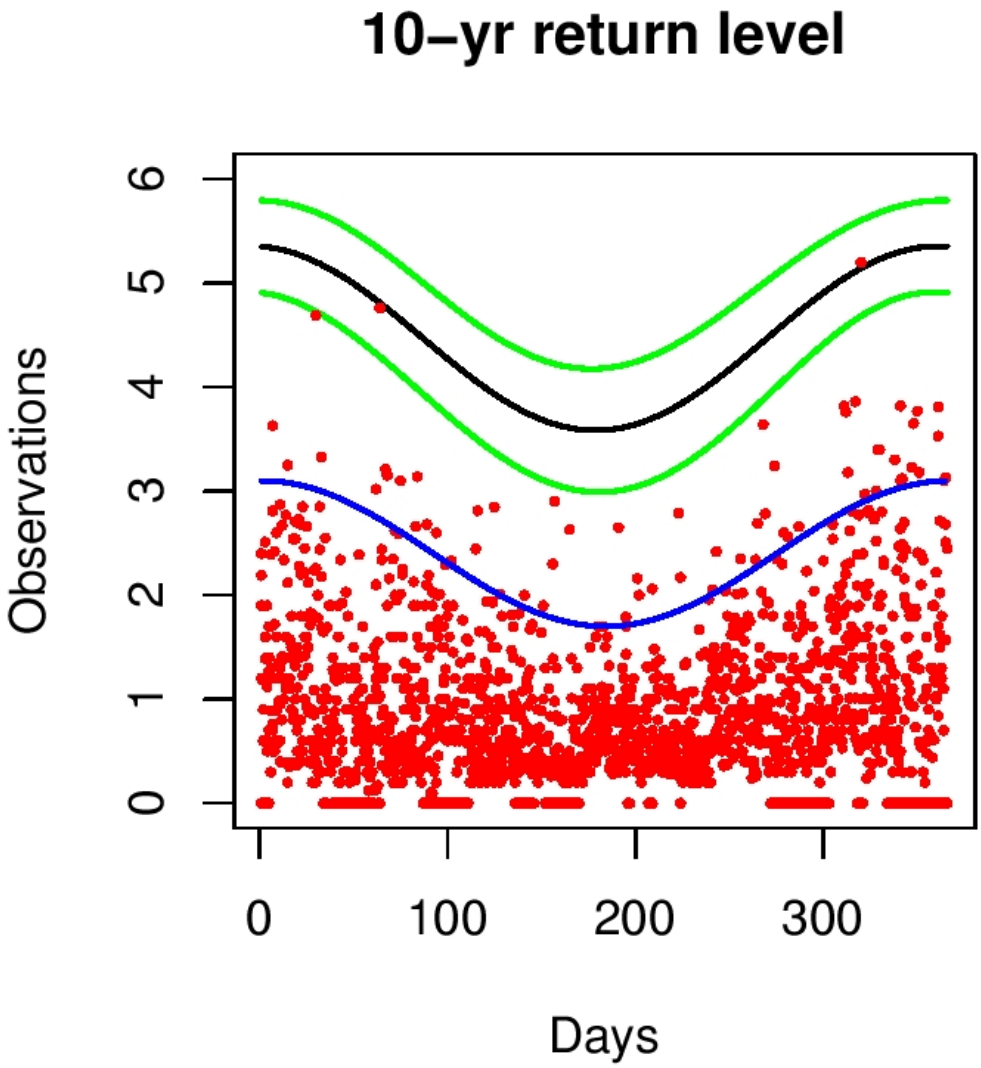

Figure 16: Seasonally-varying 10-year return level of the wave height at Ancona (black) plus σ -confidence interval (green). In red, the sequence of daily maxima of the hourly time series in Fig. 13 is plotted, together with the time-dependent threshold (3) (blue), whose coefficients are given in (10).

Lastly, seasonally dependent 10-year return levels of the waves are computed by the same simulation-based procedure as in Sec. 5. The results, presented in Fig. 16, show that larger return levels are expected in wintertime with respect to the other seasons.

4.1	0.15	0	0	0	0
-0.72	0.13	0	0	0	0
-0.24	0.07				

Table 7: Maximum likelihood estimates of the parameter vector (6) of a stationary point process model, inferred from the sequence of daily maxima of the time series in Fig. 12. The time-dependent threshold $u(t)$ as in (3) used to select the extreme values is reported in (10). The maximized log-likelihood is 71.5.

3.7	0.1	0.01	0.09	0.7	0.1
-0.8	0.19	0	0	0	0
-0.09	0.11				

Table 8: Same as Tab. 3 for a point process model with μ depending on time as in (4) and constant σ. The maximized log-likelihood is 87.6.

3.6	0.14	-0.04	0.19	0.8	0.21
-0.86	0.21	-0.05	0.15	0.09	0.17
-0.11	0.12				

Table 9: Same as Tab. 4 for a point process model with both μ and σ depending on time. The maximized log-likelihood is 87.8.

6. Conclusions

In this report, we have shown that the tide at Ancona is essentially a mixed tide with a strong diurnal constituent. The annual constituent is very important even

because tidal maxima occurring during the winter season when the meteorological conditions force strong winds that affect the water level.
Other than frequencies associated with astronomical forces, there are other effects both at lower and higher frequencies. Seiches are well visible after filtering the astronomical frequencies; it is worth noting that the spectral density of seiches is a hundredth of diurnal K1 frequency. Even seiches are due to meteorological conditions, normally Scirocco winds that excite the normal modes of the Adriatic basin. The relationship between meteorological systems affecting sea level is visible in the variability of sea level and in particular of the residual. In fact, seasonality of surge variability is well evident. Such variability has to be accounted for when defining the coastline. Thus, a coastline should be defined during summer months (July or August) in fair weather conditions.
Moreover, also the extreme analysis shows the importance of season in defining return time, that are lower in winter than in summer.

Acknowledgments

The author wish to thank the "Agenzia Nazionale per l'Ambiente e per i servizi tecnici" (APAT) that provided data of Rete Ondametrica Nazionale (RON) e Rete Mareografica Nazionale (RMN) trough internet (http://www.idromare.com). This work was funded by CINFAI trough the UE INTEREG IIIB project CADSEALAND.

Appendix A

In this appendix the amplitudes with the associated error and the signal noise ratio (snr) of the tidal constituents are shown.

tide	freq	amp	amp_err	snr
*SA	0.0001141	0.0645	0.018	12
*SSA	0.0002282	0.0285	0.019	2.3
*MSM	0.0013098	0.0033	0.012	0.078
*MM	0.0015122	0.0147	0.015	0.98
*MSF	0.0028219	0.0082	0.012	0.44
*MF	0.0030501	0.0112	0.017	0.44
*ALP1	0.0343966	0.0004	0.002	0.04
*2Q1	0.0357064	0.0005	0.002	0.065
*SIG1	0.0359087	0.0017	0.003	0.46
*Q1	0.0372185	0.0065	0.003	4.5
*RHO1	0.0374209	0.0018	0.002	0.57
*O1	0.0387307	0.0409	0.003	1.80E+02
*TAU1	0.0389588	0.0011	0.002	0.21
*BET1	0.0400404	0.0011	0.002	0.22
*NO1	0.0402686	0.0036	0.002	3.2
*CHI1	0.040471	0.001	0.002	0.21
*PI1	0.0414385	0.0049	0.003	3
*P1	0.0415526	0.0422	0.003	1.70E+02
*S1	0.0416667	0.0061	0.005	1.8
*K1	0.0417807	0.1299	0.003	2.00E+03
*PSI1	0.0418948	0.0018	0.003	0.52
*PHI1	0.0420089	0.0034	0.003	1.4
*THE1	0.0430905	0.0008	0.002	0.15
*J1	0.0432929	0.0092	0.003	9.4
*SO1	0.0446027	0.004	0.003	1.7
*OO1	0.0448308	0.0063	0.002	7.8
*UPS1	0.046343	0.0043	0.002	3.5
*OQ2	0.0759749	0.0005	0.001	0.7
*EPS2	0.0761773	0.0004	0.001	0.68
*2N2	0.0774871	0.0013	0.001	6.3
*MU2	0.0776895	0.0017	0.001	11
*N2	0.0789992	0.0121	0.001	4.40E+02
*NU2	0.0792016	0.0023	0	22
*GAM2	0.080309	0.0001	0	0.13
*H1	0.0803973	0.0006	0.001	1
*M2	0.0805114	0.0663	0.001	1.50E+04
*H2	0.0806255	0.0006	0.001	1.4

*MKS2	0.0807396	0.0004	0	0.98
*LDA2	0.0818212	0.0006	0	1.5
*L2	0.0820236	0.0027	0.001	15
*T2	0.0832193	0.0015	0.001	8.3
*S2	0.0833333	0.0355	0.001	3.90E+03
*R2	0.0834474	0.0004	0	0.77
*K2	0.0835615	0.0104	0	6.50E+02
*MSN2	0.0848455	0.0003	0	0.49
*ETA2	0.0850736	0.0009	0	3.2
*MO3	0.1192421	0.0002	0	0.56
*M3	0.1207671	0.0024	0	37
*SO3	0.122064	0.0007	0	3.6
*MK3	0.1222921	0.0003	0	0.72
*SK3	0.1251141	0.0012	0	10
*MN4	0.1595106	0.0002	0	0.39
*M4	0.1610228	0.0001	0	0.29
*SN4	0.1623326	0.0002	0	0.27
*MS4	0.1638447	0.0002	0	0.41
*MK4	0.1640729	0.0004	0	1.7
*S4	0.1666667	0.0004	0	1.5
*SK4	0.1668948	0.0002	0	0.46
*2MK5	0.2028035	0.0002	0	0.75
*2SK5	0.2084474	0.0002	0	0.75
*2MN6	0.2400221	0.0002	0	0.3
*M6	0.2415342	0.0005	0	1.8
*2MS6	0.2443561	0.0006	0	2
*2MK6	0.2445843	0.0002	0	0.56
*2SM6	0.2471781	0.0004	0	1.2
*MSK6	0.2474062	0.0003	0	1.2
*3MK7	0.2833149	0.0002	0	0.59
*M8	0.3220456	0.0001	0	0.058
*2PO1	0.0443745	0.0031	0.003	0.99

BIBLIOGRAPHY

Coles, S., 2001: An Introduction to Statistical Modelling of Extremes Values. Springer-Verlag, 208 pp.

Defant, A., 1961: Physical oceanography, Pergmon Press, Vol. 2, 590 pp.

Godin, G., 1991. The analysis of tides and currents. In: Parker, B.B (Ed.), Tidal Hydrodynamics. Wiley, New York, pp. 675–709.

Godin, G., 1972. The Analysis of Tides. University of Toronto Press, Toronto, 264pp.

Foreman, M.G.G., Crawford, W.R., Marsden, R.F., 1995. Detiding: theory and practise. In: Lynch, D.R., Davies, A.M. (Eds.), Quantitative Skill Assessment for Coastal Ocean Models. Vol. 47. Coastal and Estuarine Studies. American Geophysical Union, pp. 203–239.

Foreman, M.G.G., 1978. Manual for tidal currents analysis and prediction. Pacific Marine Science Report 78-6, Institute of Ocean Sciences, Patricia Bay, Sidney, BC, 57pp.

Hendershott, M. C., A. Speranza, 1971: Co-oscillating tide in long, narrow bays: the Taylor problem revisited. *Deep Sea Res.*, **18**, 959-980.

Jay, D.A., E. P., Flinchem, 1999. A comparison of methods for analysis of tidal records containing multi-scale non-tidal background energy. *Continental Shelf*

Research **19**, 1695–1732

Lionello, P., R. Mufato and A. Tomasin, 2005: Sensitivity of free and forced oscillations of the Adriatic Sea to sea level rise. *Climate Res.*, **29**, 23-39.

Malacic, V., D. Viezzoli, B. Cushman-Roisin, 2000: Tidal dynamics in the northern Adriatic Sea. *J. Geoph. Res.*, **105**, 265-280.

Munk, W.H., Cartwright, D.E., 1966. Tidal spectroscopy and predication. *Philosophical Transactions of the Royal Society of London*, Series **A 259**, 533–581.

Pawlowicz, R., B. Beardsley, and S. Lentz, 2002: Classical Tidal Harmonic Analysis Including Error Estimates in MATLAB using T_TIDE", *Computers and Geosciences*, **28**, 929-937.

Polli, S., 1959: La propagazione delle mare nell'Adriatico. Atti IX Convegno Ass. Geofis. Ital. Roma, 1959.

Taylor, G. I., 1921. Tidal oscillations in gulfs and rectangular basins. *Proc. Lond. Math. Soc.*, **20**, 148-181.